Kingdom of Saudi Arabia
Imam Mohammad Ibn Saud Islamic University (IMSIU)
Faculty of Sciences – Department of Physics

Comparative analysis of direct and iterative numerical methods for cancer characterization

A graduation project submitted to the Department of Physics in partial fulfillment of the requirements for the degree of Bachelor of Science in Applied Physics

by

Danah Adel Alghelani

Ghada Mubarak Almutairi

Supervisor

Dr. Maha Algarawi

IMSIU-Riyadh-KSA

May/2025

Table of Contents

Acknowledgment

.بسم الله الرحمن الرحيم، والحمد لله رب العالمين، الذي بفضله ونعمته تمكنا من إتمام هذا البحث وتحقيق نجاحه

في هذه المناسبة السعيدة، نرفع أرقى وأعذب التحيات والشكر إلى الدكتورة مها القرعاوي، التي لم تألُ جهدًا في مساعدتنا وإرشادنا خلال هذه الرحلة العلمية.

إلى دكتورتنا، نعبر عن امتناننا العميق واحترامنا الكبير، فقد كان لها تأثير عظيم في تطوير قدراتنا وإلهامنا للوصول إلى أعلى المستويات. توجيهاتها القيمة ونصائحها الثمينة كانت دليلًا لنا في كل خطوة نخطوها، ولطالما كان لديها القدرة على إبراز أفضل ما فينا وتوجيهنا نحو التميز.

نود أن نعبر أيضًا عن امتناننا العميق لأسرنا الكريمة، الذين وقفوا بجانبنا ودعمونا بكل حب وتفانٍ. بفضل دعمهم الثابت وتشجيعهم المستمر، تمكنا من تجاوز التحديات والصعاب وتحقيق هذا الإنجاز.

في هذه اللحظة الجميلة، نتوجه بكل الشكر والتقدير لكل فرد شارك بطريقة أو بأخرى في رحلتنا، ونسأل الله تعالى أن يجعل هذا البحث المتكامل خطوة نحو مستقبل مشرق ونجاح مستمر. ونسأله أن يكرم الجميع ويوفقنا جميعًا في مسيرتنا العلمية والحياتية.

.والحمد لله الذي بنعمته تتم الصالحات

List of tables

List of figures

Abstract

This research focuses on estimating chromophore concentrations in biological tissue using optical absorption data measured at three wavelengths (780 nm, 800 nm, and 860 nm) across 4225 nodes. Two numerical methods were implemented to solve the resulting linear system based on the modified Beer-Lambert law: LU Factorization and Levenberg-Marquardt. The performance of both methods was evaluated in terms of accuracy and computation time. The results clearly show that LU Factorization achieved higher accuracy and faster execution compared to Levenberg-Marquardt. This makes LU Factorization a more suitable and efficient approach for non-invasive tissue characterization and may contribute to enhancing early cancer detection techniques.

الملخص العربي

يركز هذا البحث على تقدير تركيزات الكروموفورات داخل الأنسجة البيولوجية باستخدام بيانات الامتصاص البصري المقاسة عند ثلاث أطوال موجية (780 نانومتر، 800نانومتر، و860 نانومتر) موزعة على 4225 نقطة. تم استخدام طريقتين عدديتين لحل النظام الخطي الناتج من قانون بير-لامبرت المعدل، وهما طريقة LU Factorizationوطريقة Levenberg-Marquardt تم تقييم أداء كلتا الطريقتين من حيث الدقة والسرعة الحسابية. أظهرت النتائج أن طريقة LU Factorization تفوقت بشكل واضح على طريقة-Levenberg Marquardt، حيث حققت دقة أعلى وزمنًا حسابيًا أقل. مما يجعلها الخيار الأنسب للتطبيقات التي تتطلب تحليلًا دقيقًا وسريعًا للأنسجة، ويساهم ذلك في تعزيز تقنيات الكشف المبكر عن السرطان باستخدام التصوير البصري غير الجراحي.

Chapter 1: Introduction

1.1 Introduction

Laser technology has revolutionized the medical field due to its precision and ability to minimize damage to surrounding tissues. It is widely used in various applications, including ophthalmology, dermatology, urology, and minimally invasive surgeries. In dermatology, lasers are employed for skin treatments, while in oncology, they play a crucial role in thermal therapy and tumor ablation. Laser-based techniques have also enhanced surgical procedures by making them more precise and less invasive [1].

Beyond treatment, lasers have significantly transformed noninvasive diagnostic techniques. They are particularly important in detecting and managing diseases such as brain tumors and breast cancer through photonic technologies. One of the most notable applications of lasers in medicine is cancer detection and treatment, where they offer more accurate and earlier diagnoses compared to traditional methods [2].Traditional cancer characterization relies on physical examinations, such as biopsy whether through needle aspiration or surgical extraction as well as laboratory tests (including blood and urine analyses for cancer biomarkers) and imaging techniques like Computed Tomography (CT) and Positron Emission Tomography (PET). These methods often suffer from limitations such as low accuracy, delayed detection, and unclear results, which may require further testing. Invasive procedures like biopsies carry risks and discomfort, while imaging methods expose patients to harmful radiation. To overcome these issues, laser-based optical imaging has emerged as a safer and more effective alternative, offering higher sensitivity, better contrast, and real-time monitoring, thus reducing the need for invasive biopsies and harmful radiation exposure [3].

Optical imaging techniques use laser light to generate high-resolution images of tissues, enabling earlier and more accurate tumor detection. Among these techniques, Diffuse Optical Spectroscopy (DOS) is one of the most established and widely used in clinical applications. It provides both structural and functional information by analyzing how tissues absorb and scatter light. It focuses on the absorption spectra of oxyhemoglobin and deoxyhemoglobin since changes in their concentration often indicate abnormalities. By examining tissue behavior in the 650–1000 nm near infrared range, these methods can effectively distinguish between normal and cancerous tissues. Since absorbance depends directly on the number of absorbing molecules, the concentration of each chromophore significantly affects how much light is absorbed. A highly concentrated solution will absorb light

more due to the higher number of interacting molecules, whereas a dilute solution may show little to no absorbance [4].

Building on this concept, this project focuses on solving the linear systems derived from the modified Beer-Lambert law to accurately estimate chromophore concentrations in tissue. This law defines a mathematical relationship between light absorbance and concentration, allowing us to extract quantitative data from optical measurements. In this study, we simulate phantom tissues with varying known concentrations, based on real data for normal and abnormal tissue composition. To solve the resulting linear systems, we apply both direct and iterative numerical methods specifically LU decomposition and the Levenberg Marquardt. We then compare the results in terms of accuracy (error analysis) and computational efficiency.

1.2 Laser

LASER: is an abbreviation for Light Amplification by Stimulated Emission of Radiation. This means that a laser produces and amplifies an intense beam of highly coherent, highly directional light. A laser consists of at least three components as shown in Figure (1.1).

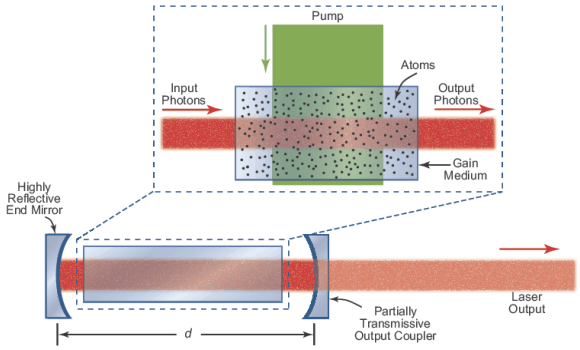

Figure (1.1): The component of the laser [6].

The first component is a gain medium that can amplify light. The second one is a pump source that creates population inversion in the gain medium. Finally, two mirrors forming an optical cavity to trap the light, the laser is the beam of light that escapes the optical cavity [5].

The laser operation is based on the principle of stimulated emission, which enables light amplification. When an atom is excited to a higher energy level (e_2), it can return to a lower energy

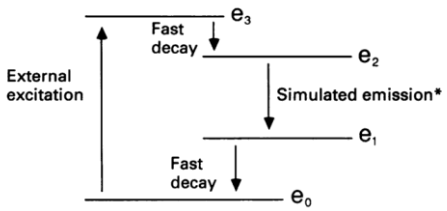

Figure(1.2): The four-level energy diagram [7].

level (e_1) by emitting a photon with energy equal to (e_2 - e_1), as shown in figure (1.2) ,Suppose an incoming photon with the same energy as energy difference between e_2 and e_1 interacts with the excited atom. In that case, it can stimulate the release of another photon that is identical in phase, direction, and wavelength to the original photon. As this process continues, more excited atoms undergo stimulated emissions, leading to a chain reaction that generates an amplified beam of coherent and directional light [6]. Because this process is not limited to a specific wavelength, lasers can be designed to operate across a wide range of wavelengths, depending on the materials and mechanisms used [7].

1.3 Laser safety

Laser radiation can be produced at nearly any wavelength between 100 nm and 1 mm, and different wavelengths can cause different effects on human skin and internal tissues. These effects depend on several factors, including the laser's wavelength, how long the skin is exposed, how powerful the beam is, and how the tissue absorbs the light. The skin contains molecules like melanin, hemoglobin, and water that absorb light in different ways. In the visible and near-infrared range (400–1400 nm), laser light can reach deeper layers of the skin, potentially affecting blood vessels and connective tissue. In the mid- and far-infrared range (1400–10,000 nm), water absorbs most of the energy, leading to more surface-level heating that can cause burns, blisters, or protein damage.

The Maximum Permissible Exposure (MPE) is the highest level of laser radiation that skin can safely be exposed to without causing harm. This safety limit is important in medical, cosmetic, and industrial laser use. MPE depends on the laser's wavelength, exposure time, laser mode (continuous or pulsed), and the exposed area. Longer exposures and higher power levels increase the risk of skin damage. MPE is measured using Power Density (W/cm²), also known as irradiance, which indicates how much laser power is delivered per unit area [8].

1.4 Mechanism of Light Interaction in Biological Tissues

When a photon enters biological tissue, it undergoes interactions governed by key optical properties absorption and scattering. Some light is reflected at the surface, while the rest refracts into the tissue and encounters scattering by cellular structures. Scattering in tissue is highly forward directed, aiding deeper light penetration. Simultaneously, some photons are absorbed by chromophores like hemoglobin and melanin, with the absorption varying by wavelength. These processes either convert photon energy into heat or trigger photochemical effects. As a result, light can be diffusely reflected or transmitted through the tissue, depending on the balance of absorption and scattering. This behavior is fundamental in imaging and diagnostic techniques like Diffuse Optical Spectroscopy [9].

Chromophores are molecules in the biological tissue that absorb light at specific wavelengths. The biological tissue contains several key chromophores that contribute to light absorption, such as oxy-hemoglobin, deoxy-hemoglobin, melanin, as well as water and lipids. Oxy-hemoglobin and deoxy-hemoglobin absorb light in the visible spectrum (500–600 nm), with a strong absorption peak around 580 nm, as shown in Figure (1.3).

In addition, water absorbs light strongly at 980 nm, while lipids absorb light at 930 nm, the process of absorption primarily depends on the concentration of chromophores and their spectral properties. Regarding scattering, it occurs due to components like collagen and elastin fibers in the tissue and is affected by the size of the scattered particles. In the deeper dermis, scattering reflects the larger collagen bundles, while in the epidermis, it reflects the smaller melanin granules. This scattering affects how light propagates through the skin, altering the way we perceive the skin's appearance. Understanding light-tissue interactions, including absorption and scattering, is crucial for identifying the optical window, which is the specific wavelength range where light penetration in biological tissues is maximized due to minimal absorption and scattering. This window typically spans from about 650 nm to 1000 nm in the near-infrared region, where key chromophores such as hemoglobin and water exhibit low absorption.

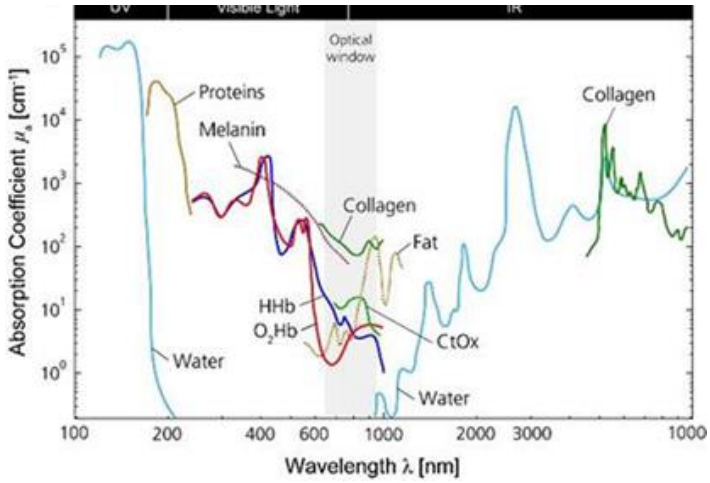

Figure(1.3): Absorption spectra of different chromophores [10].

The optical properties of tissues are light absorption and scattering. The key parameters measured are the absorption coefficient μ_a , which is a measure of how much light is absorbed by a material at a specific wavelength. It quantifies the amount of light lost per unit length as light travels through tissue. The unit of μ_a is typically expressed in (cm^{-1}) or (mm^{-1}), indicating the absorption per unit distance. Additionally, the scattering coefficient μ_s describes how light propagates within tissue [10].

1.5 The modified Beer–Lambert Law

The Beer-Lambert Law is a fundamental principle in spectroscopy that relates the absorbance of light by a solution to the concentration and the path length the light travels through the medium. Figure (1.4) illustrates this concept, where light enters the absorbing sample with an initial intensity I_0 and exits with a reduced intensity I due to absorption. The distance traveled by the light through the sample is called the path length. This setup demonstrates how the absorbance depends on both the concentration of the absorbing material and the length of the medium the light travels through. According to this law, absorbance increases proportionally with both concentration and path length. This relationship allows for the determination of substance concentrations by measuring light absorbance at a specific wavelength [11].

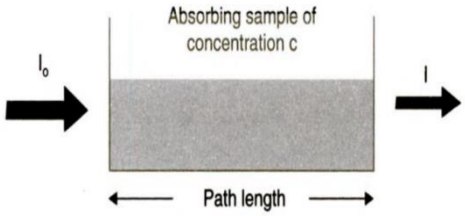

Figure (1.4): Illustration of light absorption in a sample [11].

The Beer-Lambert law that describes the attenuation of light passing through a medium is given by:

$$\boldsymbol{I = I_0 \cdot e^{-\mu_a \cdot d}} \qquad (1)$$

where $\boldsymbol{I}$ is the intensity of light passing through the medium, I_0 is the original light intensity before entering the medium, $\boldsymbol{\mu_a}$is the absorption coefficient of the medium, and $\boldsymbol{d}$ is the path length of the light within the medium. By taking the natural logarithm of both sides, we get the equation:

$$\boldsymbol{In\left(\frac{I}{I_0}\right) = -\mu_a \cdot d} \qquad (2)$$

From this equation, the relationship between absorption and concentration can be obtained, resulting in the modified Beer-Lambert law equation:

$$\boldsymbol{\mu_a = In\,(10) \cdot \varepsilon \cdot C} \qquad (3)$$

where $\boldsymbol{\varepsilon}$ is the extinction coefficient and C is the concentration of the chromophore. Based on this equation, we can relate the absorption coefficient μ_a to the chromophore concentration using the extinction coefficient.

1.6 Numerical Methods

Numerical methods continuously evolve to solve complex problems in applied and pure sciences, such as weather forecasting, disease modeling, and chemical reactions. Many of these problems require solving systems of linear equations, which arise either naturally or during computational processes. These systems involve multiple variables, and no single solution method works best for all cases. Selection depends on speed and accuracy, especially for large-scale computations where efficiency is crucial in the medical field. Numerical methods for solving mathematical problems can be approached using either direct methods, which yield a solution in a finite number of steps, or iterative methods, which produce successively better approximations of the solution.

One of the direct methods is LU Decomposition. It is a method of factorizing a square matrix A into a lower triangular matrix L and an upper triangular matrix U, such that $A = LU$. This decomposition simplifies solving linear equations by converting the original system into two simpler, direct steps: forward substitution with L and backward substitution with U. It is particularly effective for square matrices, making it an efficient approach for large systems [13].

On the other hand, Levenberg–Marquardt (LM) is an example of the iterative methods. LM algorithm is a hybrid optimization technique designed for solving even nonlinear least squares problems. LM was developed through the combined contributions of Levenberg (1944) and Marquardt (1963), the method balances the fast convergence of the Gauss–Newton algorithm with the stability of gradient descent using a damping parameter that adjusts dynamically. LM is especially robust in the presence of spars data, poor initial guesses, or ill-conditioned systems. It typically exhibits fast, near-quadratic convergence, making it highly efficient. Its straightforward implementation and stability under challenging conditions make it widely used and reliable [13].

1.7 Literature review

In a study by S.L. Jacques *et al*. researchers investigated the use of optical spectroscopy to quantify chromophore concentrations in biological tissues. By analyzing the absorption and scattering properties of light across ultraviolet to near-infrared wavelengths (250–2500 nm), the study demonstrated how diffuse reflectance spectroscopy could non-invasively measure hemoglobin, melanin, and water content in skin and brain tissue. The researchers found that wavelength-specific absorption peaks (542 nm and 577 nm for oxyhemoglobin) enabled precise differentiation between healthy and pathological tissues, such as tumors, which exhibit altered scattering coefficients. This

approach could guide the development of real-time diagnostic tools for cancer detection, as malignant tissues often show elevated hemoglobin absorption and reduced lipid content compared to normal tissue. Additionally, the study highlighted the importance of correcting for scattering effects using modified versions of the Beer-Lambert law, which is critical for accurate concentration measurements in turbid media. These findings will help us know how the tumor and healthy tissues differ in the value of their concentration [9].

Tromberg *et al*. conducted a study utilizing broadband diffuse optical spectroscopy (DOS) to non-invasively assess tissue composition and function. By combining frequency-domain photon migration with near-infrared spectroscopy, they quantitatively measured tissue absorption and scattering spectra. This approach enabled the evaluation of physiological parameters such as hemoglobin concentration, oxygen saturation, and water content, providing valuable insights into tissue health and pathology. The study highlighted the potential of DOS as a bedside monitoring tool for various clinical applications [14].

Donald E. *et al*. investigated the penetration depth of laser light at wavelengths of 808 nm and 980 nm through bovine tissue samples of varying thicknesses. Their research demonstrated that 980 nm laser light exhibited deeper tissue penetration compared to 808 nm, suggesting its suitability for therapeutic applications targeting deeper tissues. The findings underscore the importance of selecting appropriate laser wavelengths to achieve desired tissue penetration while minimizing potential damage to surrounding structures [15].

Chapter 2: Method

This chapter explains the numerical phantom that is designed to make predictions and show the performance of two types of numerical methods, as well as the numerical methods implementation used.

2.1 Design and Construction of the numerical phantom:

2.1.1 Simulation studies

Simulation studies are virtual experiments used to model how light interacts with numerical phantoms, which are tissue-like structures, in a controlled environment. This allows us to test, develop and optimize the numerical methods without the need for real experiments. This helps improve accuracy, reduce costs, and improved safety, especially since experiments on real tissues or patients may be risky, expensive, or impractical.

2.1.2 The Numerical Phantom Design

The phantom is designed as a two-dimensional circular shape with a diameter of 25 mm, representing a cross-sectional view of a cylindrical three-dimensional model of a small animal, such as a laboratory rat, as shown in figure (2.1).

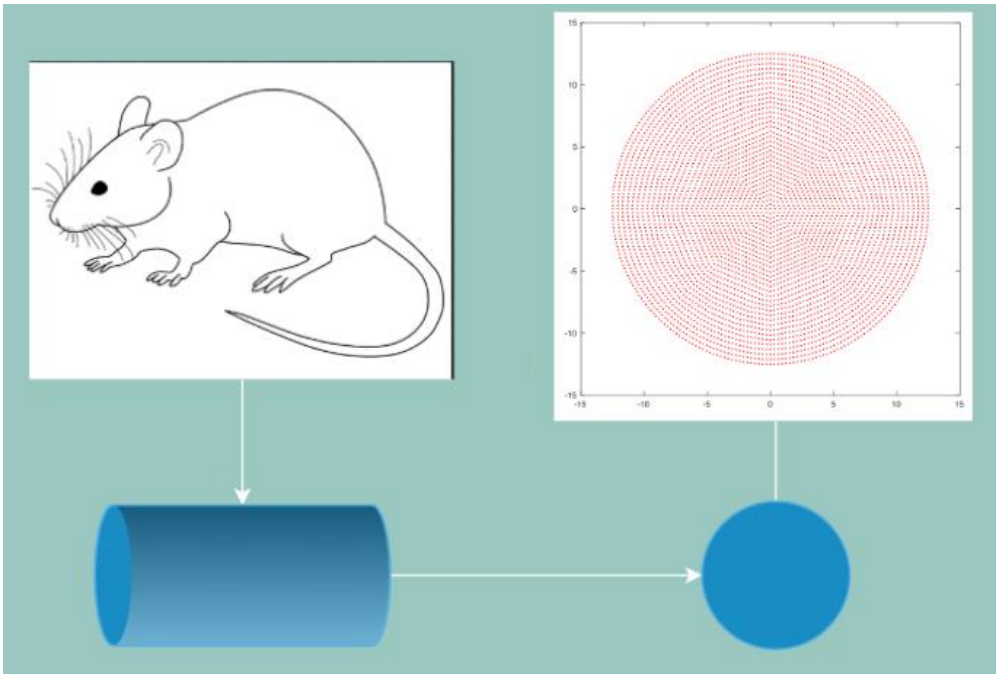

Figure (2.1): This figure shows the process of visualizing the phantom starting by sizing a small laboratory rat to cylinder then taking a cross section and then making a mesh representing the cross section with 4225 nodes.

2.1.3 Tumor size and placement

The tumor will have a diameter of 4 mm, which is appropriate for the scale of the phantom. It will be positioned at the center of the phantom, deep within the cylindrical model, to simulate a tumor located further from the surface, as shown in figure (2.2).

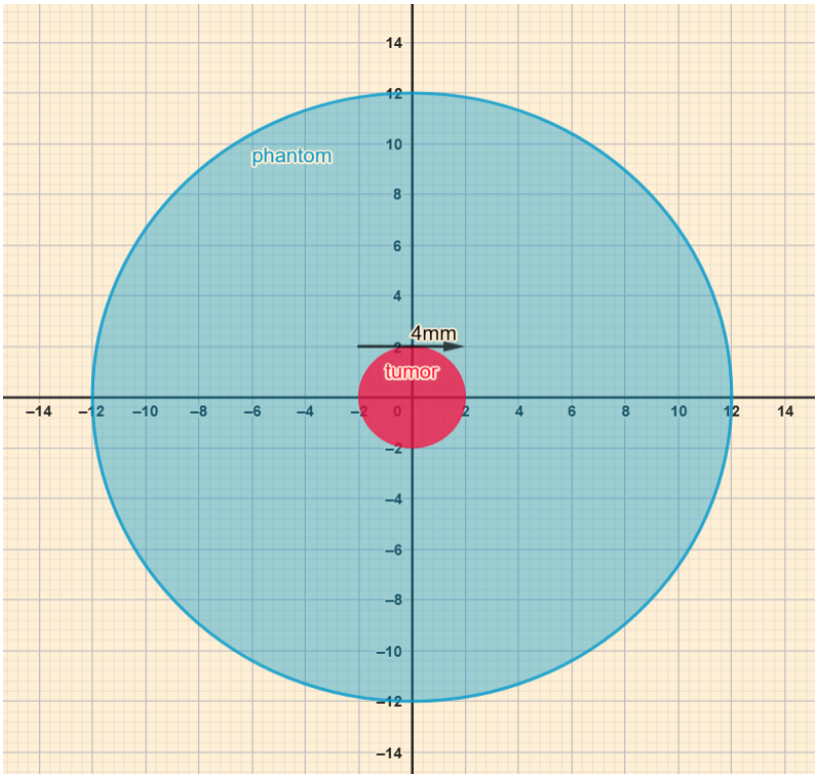

Figure (2.2): A graphical representation of the tumor placement and size within the phantom cross section.

2.1.4 Chromophore Selection

There will be three (Dye 1, Dye 2, and Dye 3), representing chromophores in biological tissue with different concentrations. The chromophores representing the blood inside the tumor will have a higher absorption compared to the surrounding tissue. Two dyes will be incorporated within the tumor to simulate the presence of blood (Dye 1 and Dye 2). The background will contain only one chromophore representing a mixture of water and fat, Dye 3.

2.1.5 Lasers and laser Parameters

There are three lasers used in this experiment, the three lasers having wavelengths of (780, 808, 860 nm). For each of the three laser wavelengths, the tissue was illuminated from four different directions, with each exposure lasting 10 seconds. The location of lasers is shown in Figure (2.3).

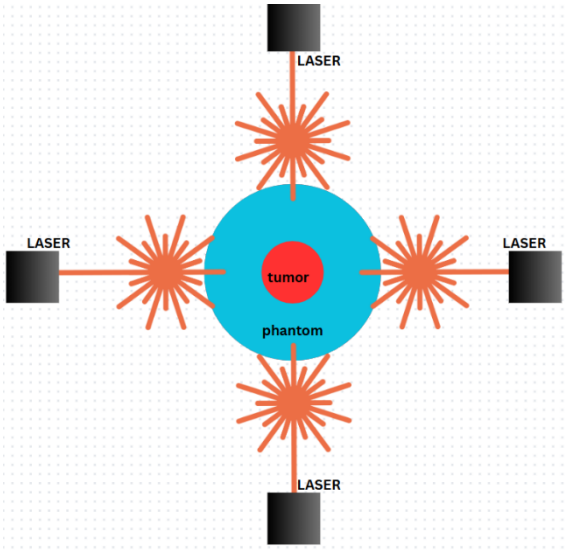

Figure (2.3): Laser's location note that they are all the same wavelengths.

We specifically chose these wavelengths because each dye used (Dye 1 and Dye 2) has its highest absorption peak at one of them. While Dye 3 has approximately constant absorption spectrum with wavelength, as shown in figure (2.4).

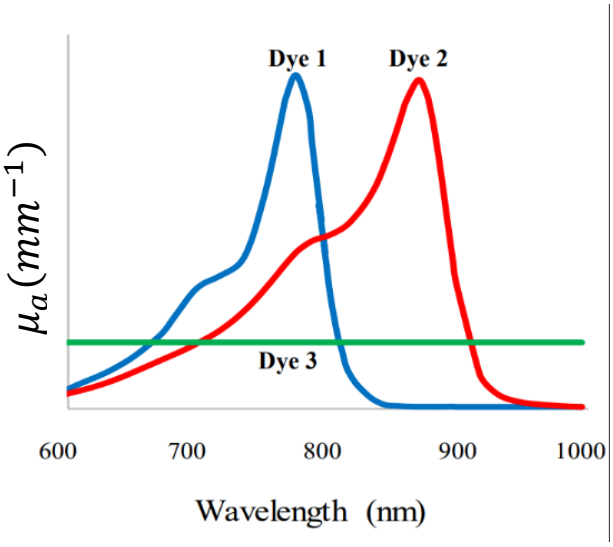

Figure (2.4): Dyes spectra [16].

In Table (2.1) is a summary of the extinction coefficients of the three dyes at the utilized wavelengths.

Table (2.1): Extinction Coefficients of Chromophores at Each Wavelength Based on Known Concentrations

Chromophores	ε at 780(nm)	ε $at\ 800(nm)$	ε $at\ 860(nm)$	Concentration%
Dye (1)	0.011	0.004	0.002	2
Dye (2)	0.024	0.025	0.045	0.5
Dye (3)	0.109	0.109	0.109	0.04

The modified Beer–Lambert Law was employed to calculate the absorption coefficients (μ_a) at wavelengths 780 nm, 800 nm, and 860 nm based on the known extinction coefficients of the chromophore dyes and their respective concentrations, Table (2.2).

Table (2.2): Absorption coefficient at each wavelength.

$\boldsymbol{\mu_a(mm^{-1})}$ **at each** $\boldsymbol{\lambda}$	$\boldsymbol{\lambda = 780(nm)}$	$\boldsymbol{\lambda = 800(nm)}$	$\boldsymbol{\lambda = 860(nm)}$
Dye (1)	0.0490	0.0170	0.0070
Dye (2)	0.0280	0.0290	0.0520
Dye (3)	0.0100	0.0100	0.0100

2.2 Mathematical Framework

In this project, the recovered absorption coefficient data at three different wavelengths were used to create a system of equations for calculating chromophore concentrations at these wavelengths. The system of equations formed consists of three equations as follows:

$$\begin{aligned} \varepsilon_{11} \cdot C_1 + \varepsilon_{12} \cdot C_2 + \varepsilon_{13} \cdot C_3 &= \mu_1 \\ \varepsilon_{21} \cdot C_1 + \varepsilon_{22} \cdot C_2 + \varepsilon_{23} \cdot C_3 &= \mu_2 \\ \varepsilon_{31} \cdot C_1 + \varepsilon_{32} \cdot C_2 + \varepsilon_{33} \cdot C_3 &= \mu_3 \end{aligned} \quad (4)$$

2.2.1 LU method and implementation.

The system of linear equations derived from the modified Beer-Lambert Law was used to calculate the chromophore concentrations (C_1, C_2, and C_3) across 4225 nodes. The system is based on the extinction coefficient matrix A, defined as:

$$A = \ln(10) \cdot \varepsilon \qquad (5)$$

where **ε** contains the extinction coefficients of three components (Dye 1, Dye 2, Dye 3) at three different wavelengths (780 nm, 800 nm, and 860 nm). Each column in the matrix corresponds to one component, while each row corresponds to a specific wavelength. The modified Beer-Lambert Law in its metrics form is written as follows:

$$\begin{bmatrix} \mu_{a1} \\ \mu_{a2} \\ \mu_{a3} \end{bmatrix} = \ln(10) \cdot \begin{bmatrix} \varepsilon_{11} & \varepsilon_{12} & \varepsilon_{13} \\ \varepsilon_{21} & \varepsilon_{22} & \varepsilon_{23} \\ \varepsilon_{31} & \varepsilon_{32} & \varepsilon_{33} \end{bmatrix} \cdot \begin{bmatrix} C_1 \\ C_2 \\ C_3 \end{bmatrix} \qquad (6)$$

To solve the system of equations, LU Factorization was applied. This method involves decomposing the extinction coefficient matrix A into two triangular matrices: a lower triangular matrix L and an upper triangular matrix U, such that $A = L \cdot U$ once the matrix is decomposed, the solution proceeds in two stages. First, forward substitution is used to solve the equation as in (7):

$$L \cdot y = \mu$$

$$\begin{bmatrix} 1 & 0 & 0 \\ \ell_{21} & 1 & 0 \\ \ell_{31} & \ell_{32} & 1 \end{bmatrix} \cdot \begin{bmatrix} y_1 \\ y_2 \\ y_3 \end{bmatrix} = \begin{bmatrix} \mu_{a1} \\ \mu_{a2} \\ \mu_{a3} \end{bmatrix} \qquad (7)$$

which yields an intermediate vector y. Then, backward substitution is applied to solve the equation as in (8):

$$U \cdot C = y$$

$$\begin{bmatrix} U_{11} & U_{12} & U_{13} \\ 0 & U_{22} & U_{23} \\ 0 & 0 & U_{33} \end{bmatrix} \cdot \begin{bmatrix} C_1 \\ C_2 \\ C_3 \end{bmatrix} = \begin{bmatrix} y_1 \\ y_2 \\ y_3 \end{bmatrix} \qquad (8)$$

resulting in the final values of the chromophore concentrations C_1, C_2, C_3. This approach ensures a stable and accurate solution for determining chromophore distributions from the absorption data.

2.2.2 Levenberg -Marquardt method implementation

In the MATLAB simulation, we estimated chromophore concentrations using the Levenberg–Marquardt method. The Jacobian matrix was defined by the extinction coefficients. The residual was calculated as the difference between the calculated absorption, which is the product of the extinction coefficients matrix and the concentration vector, and the recovered absorption coefficients. We started the algorithm using 100 iterations as a limit, the concentration initial values are set to zero to be closer to the real values for faster convergence. The damping parameter is set to 0.001 to control the balance between stability and speed, when damping value is small, the method behaves more like Gauss–Newton, converging quickly near the solution. When the damping is high, it acts more like gradient descent, which is safer when far from the solution but slows down convergence.

The equation (9) is a visual for the formula used in the code

$$\boldsymbol{C_{new} = C_{old} - (\varepsilon^T \varepsilon + \lambda I)^{-1} \varepsilon^T r} \qquad (9)$$

Where $\boldsymbol{C_{new}}$is the updated value of concentration. $\boldsymbol{C_{old}}$ ls the previous value of concentration. $\boldsymbol{\varepsilon}$ is the extension coefficient matrix. $\boldsymbol{\varepsilon^T}$ is the transpose extension coefficient matrix. $\boldsymbol{\lambda}$ is the damping factor. $\boldsymbol{I}$ is the identity matrix. And $\mathbf{r}$ is the residual which is calculated in equation (10) as:

$$\mathbf{r = \varepsilon C_{old} - \mu_a} \qquad (10)$$

where $\boldsymbol{\mu_a}$ is the absorption coefficient recovered from the simulation study and $\boldsymbol{\varepsilon C_{old}}$ is the calculated absorption coefficient.

Chapter 3: Result

This chapter begins by illustrating the temperature distribution and how the absorption coefficient affects the tumor differently from the background. We then compare the LU Factorization and Levenberg-Marquardt methods result of the concentration in terms of speed and accuracy for estimating chromophore concentrations.

3.1 Temperature maps

In optical imaging simulations, lasers are used to deliver light energy into a biological medium represented by a mesh of nodes. Each node corresponds to a spatial point in the tissue model and has specific optical properties such as the absorption coefficient. When the laser light interacts with the tissue, energy is absorbed differently across nodes depending on their chromophore concentrations. This absorbed energy is then converted into heat, leading to a rise in temperature at each node. The result is a temperature map that reflects how the light energy is distributed and absorbed across the tissue. By analyzing these temperature maps, especially in regions like tumors versus healthy areas, researchers can gain insights into how light behaves in the tissue and how this behavior can help in detecting abnormalities. Figure (3.1) shows the temperature distribution map resulting from light absorption in the tissue using a 780 nm ,800 nm and 860 nm wavelength laser. It can be observed that the temperature at the tumor center is higher compared to the surrounding areas, indicating a higher absorption coefficient in that region. Additionally, the laser source regions are easily identifiable, as they emit bright illumination surrounding the central tumor.

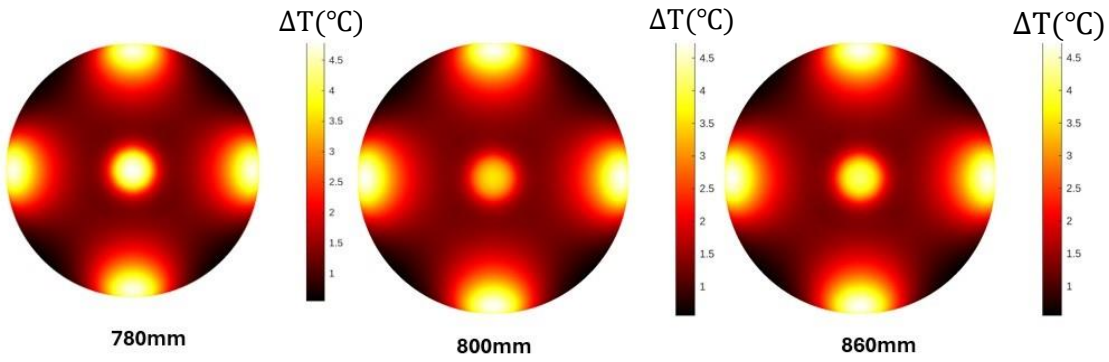

Figure (3.1): Temperature map showing higher heat in the tumor at the center due to stronger light absorption while the lasers source reigion is also illuminated.

3.1.1 Absorption maps

The Absorption maps were founded from the temperature maps. We convert them into absorption maps through a written code at each of the three wavelengths (780nm 800nm 860nm) then used the resultant absorption in our calculation to find the concentration for each Dye.

3.2 Results of the Numerical Methods

Two parameters have been used to compare the two numerical methods, the accuracy and calculation speed. To evaluate the accuracy of our method, we calculated the absolute errors inside the tumor region and outside to show how close the estimated concentration was to the true value using the formula:

$$\text{Error} = |Real - Experiment| \times 100$$

For the processing time, we used the tic and toc functions in MATLAB to measure how long the method takes to run. Tic starts a timer right before the calculation begins, and toc stops the timer and displays the elapsed time once the calculation finishes. This helps us evaluate the speed and efficiency of our method.

3.2.1 LU Factorization Method Result

The LU Factorization method was used to solve the linear system formed by the extinction coefficient matrix and the absorption coefficient data. The matrix was decomposed into lower (L) and upper (U) triangular matrices, allowing forward and backward substitution to determine the concentration values at each of the 4225 nodes. The tumor region was defined by the circular condition which identified 121 nodes inside the tumor and 4104 outside.

$$,y^2 + x^2 = 2^2$$

As shown in figure (3.2) the distribution of concentration results of Dye (1) and Dye (2) as the result of the LU method showed a clear contrast between tumor and non-tumor regions.

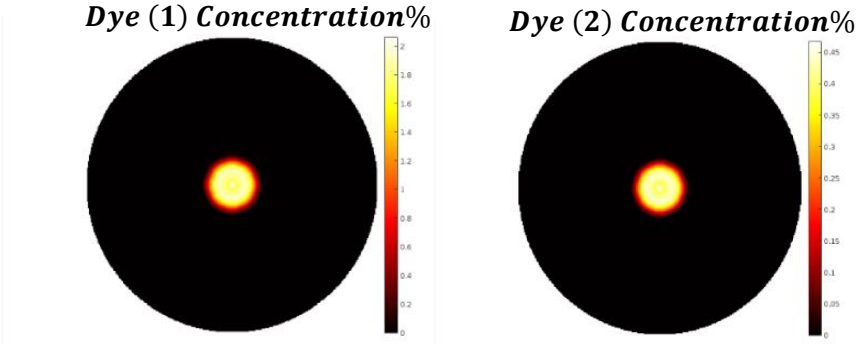

Figure (3.2): distribution of chromophore concentration of dye (1) and dye (2) By the LU method.

Table (3.1:) The result values of the LU method

Concentrations	Average Inside tumor	Average Outside tumor	Error percentage inside	Error percentage outside
Dye1	1.644	0.005	35.559%	0.531%
Dye2	0.377	0.001	12.299%	0.1203%
Dye3	0.043	0.040	4.284%	0.0001%
Calculation speed	0.001 seconds to calculate all 4225 nodes			

Table (3.1) shows the average estimated concentrations of chromophores obtained using the LU Factorization method. It also includes the corresponding error percentages, which help assess the method's reliability and precision in recovering the actual concentration values. Additionally, the LU Factorization method demonstrates high computational efficiency, making it suitable for applications requiring fast real-time or near-real-time processing.

3.2.2 Levenberg Marquardt method Result

The Levenberg-Marquardt method approached the problem as linear least squares optimization. The extinction coefficient matrix served as the Jacobian, and the residual was defined as the difference between estimated and measured absorption coefficients. A damping parameter of 0.001 was used to stabilize and control the step size. The method iteratively adjusted the concentration values to minimize the residual for each node over all the 4225 nodes.

As with the LU method, the tumor region was defined using the circle condition. The resulting concentration seen in figure (3.3) showed elevated values within the tumor region and lower values

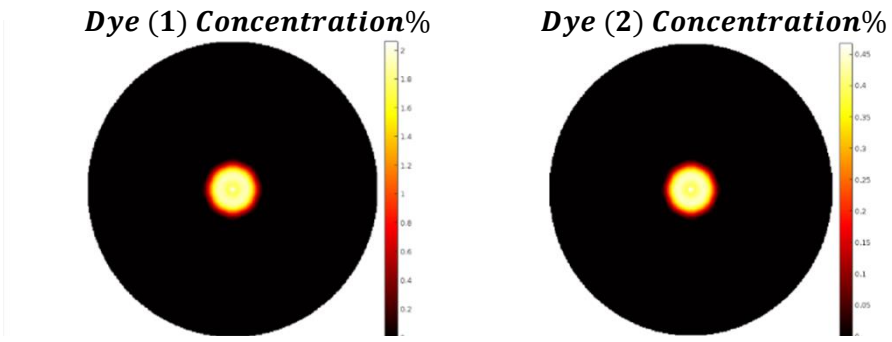

Figure (3.3): distribution of chromophore concentration of dye (1) and dye (2). By the Levenberg Marquardt method

outside, confirming the algorithm's sensitivity to localized absorption.in dye 1 and dye 2.

Table (3.2): The concentration values and analysis of the Levenberg Marquardt

Concentrations	Average Inside tumor	Average Outside tumor	Error percentage Inside	Error percentage outside
Dye1	1.642	0.007	35.740%	0.643%
Dye2	0.377	0.001	12.349%	0.154%
Dye3	0.043	0.040	4.308%	0.020%
Calculation speed	0.064 seconds to calculate 4225 nodes			

Table (3.2) presents the concentration results obtained using the Levenberg-Marquardt method. The method delivered reliable concentration estimates with smooth spatial distribution. Although it took more time than the LU method to calculate iteratively each node, it maintained robustness in the presence of residual error and provided the same Level of accuracy as the LU method.

3.2.3 Comparison of the Two Methods

Both methods effectively identified the tumor region by producing higher chromophore concentrations at its center. However, the LU Factorization method demonstrated superior performance in terms of speed and accuracy. It achieved similar error percentages to the other method and completed the calculations 48 times faster than the Levenberg, making it more suitable for real-time or large-scale applications. In contrast, the Levenberg-Marquardt method, while slightly less accurate and significantly 48 times slower, offered flexibility and stability in cases with more complex residual structures or near-singular systems.

Conclusion

This study compared LU Factorization and the Levenberg–Marquardt algorithm for estimating chromophore concentrations in biological tissues. The results demonstrated that LU Factorization outperformed Levenberg–Marquardt in both computational speed and estimation accuracy. LU efficiently solved linear systems with reduced computational time, making it well-suited for real-time medical imaging applications. In contrast, the Levenberg–Marquardt method is more effective in cases where the number of chromophore concentrations dose not match the number of Lasers, leading to a non-square system matrix. In such scenarios, Levenberg–Marquardt offers greater flexibility and adaptability, whereas LU Factorization, which is optimized for square systems, is less applicable. However, Levenberg–Marquardt generally requires more iterations and that takes more computation time, and its performance is more sensitive to initial parameter estimates. LU Factorization, by contrast, provided a direct, stable, and reliable solution, even for large-scale data sets. Overall, LU Factorization proved to be the superior method in terms of performance, robustness, and precision. These findings underscore LU as a preferred numerical technique for accurate and efficient cancer characterization using optical imaging data.

REFERENCES

[1] D. R. Vij and K. Mahesh, Ed., *Medical Applications of Lasers*. Springer US, 2002. doi: 10.1007/978-1-4615-0929-5.

[2] H. Jelínková, "Introduction: the history of lasers in medicine," in *Lasers for Medical Applications*, Elsevier, 2013, pp. 1–13. doi: 10.1533/9780857097545.1.

[3] A. Pulumati, A. Pulumati, B. S. Dwarakanath, A. Verma, and R. V. L. Papineni, "Technological advancements in cancer diagnostics: Improvements and limitations," *Cancer Rep*, vol. 6, no. 2, Feb. 2023, doi: 10.1002/cnr2.1764.

[4] M. Solomon, Y. Liu, M. Y. Berezin, and S. Achilefu, "Optical imaging in cancer research: Basic principles, tumor detection, and therapeutic monitoring," Jul. 2011. doi: 10.1159/000327655.

[5] Prof. Dr. Frank Träger, "Springer Handbook of Lasers and Optics," Apr. 2012.

[6] A. J. Welch, J. H. Torres, and W. F. Cheong, "Laser physics and laser-tissue interaction.," *Tex Heart Inst J*, vol. 16, no. 3, pp. 141–9, 1989.

[7] K. Shimoda, *Introduction to Laser Physics*, vol. 44. Berlin, Heidelberg: Springer Berlin Heidelberg, 1986. doi: 10.1007/978-3-540-38954-5.

[8] D. A. Corder, D. R. Evans, and J. R. Tyrer, "An intelligent maximum permissible exposure meter for safety assessments of laser radiation," *Opt Laser Technol*, vol. 28, no. 6, pp. 409–415, Sep. 1996, doi: 10.1016/0030-3992(96)00025-4.

[9] S. L. Jacques, "Erratum: Optical properties of biological tissues: A review (Physics in Medicine and Biology (2013) 58)," Jul. 21, 2013. doi: 10.1088/0031-9155/58/14/5007.

[10] M. J. C. van G. Ashley J. Welch, Ed., *Optical- Response of Laser-Irradiated Tissue*. New York, 1995.

[11] *Principles of Biotechnology and Genetic Engineering*. 2010.

[12] E. Agullo *et al.*, "LU factorization for accelerator-based systems," in *2011 9th IEEE/ACS International Conference on Computer Systems and Applications (AICCSA)*, IEEE, Dec. 2011, pp. 217–224. doi: 10.1109/AICCSA.2011.6126599.

[13] J. Nocedal and S. J. Wright, "Numerical Optimization Second Edition."

[14] B. Tromberg, "Broadband Diffuse Optical Spectroscopy", Accessed: May 07, 2025. [Online]. Available: https://grantome.com/grant/NIH/U54-CA105480-01-1

[15] D. E. Hudson, D. O. Hudson, J. M. Wininger, and B. D. Richardson, "Penetration of laser light at 808 and 980 nm in bovine tissue samples," *Photomed Laser Surg*, vol. 31, no. 4, pp. 163–168, Apr. 2013, doi: 10.1089/pho.2012.3284.

[16] M. Algarawi *et al.*, "High-resolution chromophore concentration recovery using multi-wavelength photo-magnetic imaging," *https://doi.org/10.1117/12.2504310*, vol. 10871, pp. 36–43, Feb. 2019, doi: 10.1117/12.2504310.